Optical phonons in the wurtzstannite Cu_2ZnGeS_4 semiconductor: Polarized Raman spectroscopy and first-principle calculations

M. Guc,[1] A. P. Litvinchuk,[2] S. Levcenko,[3] V. Izquierdo-Roca,[4] X. Fontané,[4] M. Ya. Valakh,[5]
E. Arushanov,[1] and A. Pérez-Rodríguez[4,6]

[1]*Institute of Applied Physics, Academy of Sciences of Moldova, Chisinau MD 2028, Moldova*

[2]*Texas Center for Superconductivity and Department of Physics, University of Houston, Houston, Texas 77204-5002, USA*

[3]*Helmholtz Zentrum Berlin fur Materialien und Energie, Berlin D-14109, Germany*

[4]*IREC, Catalonia Institute for Energy Research, Sant Adria del Besos (Barcelona) 08930, Spain*

[5]*Institute of Semiconductor Physics, National Academy of Sciences of Ukraine, Kiev 03028, Ukraine*

[6]*IN²UB, Departament d'Electronica, Universitat de Barcelona, Barcelona 08028, Spain*

The vibrational properties of the wurtzstannite Cu_2ZnGeS_4 are studied experimentally by polarized Raman scattering in off-resonant and resonant conditions and theoretically by *ab initio* lattice dynamics calculations. Twenty-nine modes from 45 Raman active theoretically predicted have been experimentally detected and identified, including polar $A_1(TO)$, $A_1(LO)$, and $B_1(TO+LO)/B_2(TO+LO)$ and nonpolar A_2 symmetry phonon modes from measurements on (2 1 0) and (0 0 1) crystallographic planes of Cu_2ZnGeS_4 single crystals. The lattice dynamics calculations provide a full picture of the zone center phonon spectrum and allow the assignment of experimentally observed lines to first- and second-order lattice vibrations. Using resonance Raman conditions, a strong enhancement of the $A_1(LO)$ modes with the highest longitudinal-transversal spiting is observed.

PACS number(s): 78.30.Am, 63.20.−e

I. INTRODUCTION

Among copper quaternaries chalcogenides, the Cu_2ZnGeS_4 (CZGeS) semiconductor adopts both tetragonal and orthorhombic (wurtzstannite) crystal structures [1–5]. In early studies, by addition of the Mn magnetic ions to wurtzstannite CZGeS, a weaker antiferromagnetic interaction and a higher magnetization than for the II-VI diluted magnetic semiconductors were attained [6,7]. Recently, the tetragonal CZGeS has been applied as a photofunctional material for hydrogen evolution [8] as well as a nanoparticle precursor for fabrication $Cu_2ZnSn_{1-x}Ge_x(S,Se)_4$ thin film solar cells through the selenization treatment [9,10]. CZGeS and closely related quaternary compounds such as $Cu_2ZnSnS(Se)_4$ have a strong potential interest for the development of sustainable thin film photovoltaic technologies that, in contrast with more mature $Cu(In,Ga)(S,Se)_2$ chalcopyrite ones, do not include scarce elements. This provides a strong interest in the deepening knowledge of their fundamental properties [11–13], including their optical [14,15] and vibrational properties [16,17].

The wurtzstannite CZGeS unit cell (space group P$mn2_1$) has two formula units and consists of 16 atoms [1]. The unit cell is derived by the doubling of an orthohexagonal wurtzite cell in the *a* direction. The current understanding of the physicochemical properties of CZGeS has been gained mainly from the x-ray diffraction (XRD) [1–5] and first-principles theory [13,15,18] studies. Recently absorption [19], ellipsometry [20], modulation reflection [19], and photoluminescence [21] of CZGeS have been reported. The available information on vibrational properties is limited to experimental far infrared [22] and unpolarized Raman scattering investigations [21,23] where no assignments of the reported phonon modes were done. However, to better understand basic properties of the phonon spectrum and perform an assignment of the observed lines to specific lattice eigenmodes, it is important to perform a set of polarization measurements with varied incident and scattered light polarizations on the high quality crystal faces [24]. Although theoretical electronic structure calculations were recently done for the CZGeS [13,15,18], they do not contain information on lattice vibrations.

Here we present the results of a systematic study of the phonon structure in Cu_2ZnGeS_4 semiconductor by polarized Raman scattering, resonance Raman scattering, and lattice dynamics *ab initio* calculations. We examine and analyze calculated zone center phonons with those derived from the combined polarization Raman measurements on the basal (2 1 0) and (0 0 1) crystal facets of Cu_2ZnGeS_4 single crystals. Finally, the resonance enhancement and temperature effects on the phonon spectrum were studied and discussed.

II. EXPERIMENTAL DETAILS

The CZGeS single crystals were grown by chemical vapor transport using iodine as a transporter. The pure elements of Cu, Zn, Ge, and S in the stoichiometric proportion were placed in evacuated ampoule together with 5 mg/cm^3 of iodine. The growth process was performed in the vertical two zone furnace during 14 days, and the evaporation and growth temperature were 800 °C and 750 °C, respectively. Chemical composition was investigated using energy dispersive x-ray analysis, which showed the composition of selected sample close to stoichiometry (Cu:Zn:Ge:S = 24.2:11.8:11.9:52.1, all values in at.%). The crystal orientation was determined by rotating orientation XRD method, and it revealed that the normal basal plane is (2 1 0), and the long edge of the crystal platelet is parallel to the *c* axis.

Raman spectra were measured using a LabRam HR800-UV Horiba Jobin Yvon spectrometer with solid state laser (line 785 nm) being the laser excitation source. All Raman measurements were performed in the backscattering configuration. The resonant Raman (RR) spectra were carried out at room and

low (80 K) temperatures with the Ar+ laser (line 514.5 nm) as an excitation source. More detailed experimental conditions were described in Refs. [25,26].

III. LATTICE DYNAMICS CALCULATIONS

Cu_2ZnGeS_4 crystallizes in the orthorhombic wurtzstannite structure (space group #31, $Pmn2_1$) with the lattice parameters $a = 7.5090$, $b = 6.4790$, and $c = 6.1920$ Å [3]. Our total energy calculations, which will be discussed below in more detail, show that wurtzstannite phase of Cu_2ZnGeS_4 is indeed energetically more favorable in comparison with the tetragonal stannite and kesterite structural modification.

The density functional theory (DFT) calculations of the electronic ground state and vibrational properties of Cu_2ZnGeS_4 of wurtzstannite structural modification were performed within the generalized gradient approximation using Perdew-Burke-Ernzerhof local functional [27], as implemented in the CASTEP code [28]. Norm-conserving pseudopotentials were used. Prior to performing calculations the structure was relaxed while keeping lattice parameters fixed and equal to the experimentally determined ones so that forces on atoms in the equilibrium position did not exceed 3 meV/A. The electronic band structure calculations of Cu_2ZnGeS_4 clearly reveal their semiconducting behavior, and fixed electron occupancy constrains were imposed on the self-consistent field energy minimization as a prerequisite for using the linear response scheme [29] in the phonon calculations, which treats atomic displacements as perturbations. Further, the electric field response along different crystallographic directions was evaluated, which allows calculation of longitudinal optical (LO) phonon frequencies at the Brillouin-zone center in addition to transverse optical (TO) modes.

The crystallographic unit cell (Fig. 1) of DFT-relaxed Cu_2ZnGeS_4 structure with lattice parameters mentioned above and the cation-anion bond lengths are listed in the Table I. Calculated zone center vibration modes positions of wurtzstannite type Cu_2ZnGeS_4 are summarized in Table II.

IV. PHONON MODE ASSIGNMENT

The group theoretical analysis of wurtzstannite type structure Cu_2ZnGeS_4 yields 45 Raman active modes at the center of Brillouin zone [22]:

$$\Gamma = 13A_1 \oplus 10A_2 \oplus 9B_1 \oplus 13B_2. \tag{1}$$

FIG. 1. (Color online) Crystallographic unit cell of orthorhombic tetrahedrally coordinated Cu_2ZnGeS_4 (space group #31). Sulphur tetrahedra are shown around lattice cations. S ions are shown in yellow, Ge are shown in light blue, Zn are shown in dark blue, and Cu are shown in orange.

As the structure is not centrosymmetric, polar modes of A_1, B_1, and B_2 symmetry are simultaneously infrared active.

To investigate the symmetry of the vibrational modes of Cu_2ZnGeS_4 single crystals, we performed Raman scattering measurements from the two well-defined crystallographic planes: (2 1 0), the biggest plane of the investigated sample, and (0 0 1), the plane perpendicular to the sample growth direction [0 0 1] (Fig. 2). For the (0 0 1) plane, it is natural to use a "standard" coordinate system, where X, Y, and Z axes lie along the [1 0 0], [0 1 0], and [0 0 1] crystal directions, respectively. In the case of the (2 1 0) plane, it is more convenient instead to use $(X'Y'Z)$ system, where the X' axis is normal in the (2 1 0) plane and Y' is along the [−2 1 0] direction. For clarity, both coordinates systems are also shown in Fig. 2. Following a simple coordinate system transformation, it is easy to show [25] that scattering selection rules for all used experimental configurations should be those listed in Table III. Here we used standard Raman tensors for the point group C_{2v} [30] in the case of the (0 0 1) plane and for those reported in Ref. [25] for the (2 1 0) plane.

A. A symmetry modes

The $A_1(TO)$, $A_1(LO)$, and A_2 symmetry modes could be identified using the spectra measured in configurations $\langle \overline{X'}|ZZ|X' \rangle$, $\langle \overline{Z}|XX|Z \rangle$, and $\langle \overline{Z}|XY|Z \rangle$, respectively, as

TABLE I. Crystallographic unit cell of DFT-relaxed Cu_2ZnGeS_4 in wurtzstannite-type structure and cation-anion bond lengths.

Atom	Wyckoff position	x/a	y/b	z/c	Bond lengths	
Cu	4b	0.75265	0.67580	0.17839	Ge–S1	2.2278
Zn	2a	0	0.84203	0.66721	Ge–S2	2.2376
					Ge–S3	2.2401 (two bonds)
Ge	2a	0	0.17054	0.17025	Zn–S2	2.3683
S1	2a	0	0.84538	0.05324	Zn–S1	2.3904
					Zn–S3	2.4065 (two bonds)
S2	2a	0	0.18374	0.53136	Cu–S3	2.2903
S3	4b	0.73909	0.65920	0.54749	Cu–S2	2.2926
					Cu–S1	2.2929
					Cu–S3	2.3176

TABLE II. Calculated and experimental zone center phonon frequencies. The peak symmetry assignment was done based on polarization Raman mode behavior. For A_1 symmetry modes, the TO and LO phonons were found in Raman spectra measured from (2 1 0) and (0 0 1) planes, respectively. The enhanced modes which appear only in resonance Raman spectra are indicated in bold, and they are related to LO phonons of B_1/B_2 symmetry modes.

Theory	Experiment	Theory	Experiment	Theory	Experiment	Theory	Experiment
A_1 TO/LO	A_1 TO/LO	A_2	A_2	B_1 TO/LO	B_1	B_2 TO/LO	B_2
59/59	–	45	–	64/68	–	84/84	–
83/83	83/84	57	–	80/80	–	95/95	–
106/107	99/101	78	–	110/110	111	106/106	–
113/113	114/–	99	100	181/182	175	154/154	–
185/185	178/179	167	167	283/290	**277**	163/164	**161**
188/188	–	279	274	290/292	–	192/192	**184**
283/287	272/272	284	287	299/307	–	290/291	**288**
299/306	288/291	306	302	327/329	**327**	308/311	–
310/315	309/311	325	328	381/399	383	318/321	**314**
332/336	330/333	383	376			324/331	–
358/358	361/362					364/365	–
390/391	386/388					393/394	**392**
396/410	394/407					403/415	**416**

follows from Table III. These spectra are plotted in Fig. 3(a) with indication of different modes by vertical dashed lines. The obtained frequencies of A_1(TO), A_1(LO), and A_2 symmetry modes are listed in Table II and agree well with calculated ones: for the majority of modes, the relative deviation of calculated frequencies from experiment did not exceed 3%, and only for the A_1 (TO/LO) peaks experimentally observed at 99/101, 272/272, and 288/291 cm^{-1} is a higher error observed. However, even in these cases, relative differences are below 7%. This points out a reasonable agreement between experimental and calculated sets of values. The region 200–370 cm^{-1} of the most intense modes is enlarged to show in more detail Lorentzian functions used for a decomposition of $\langle \overline{Z}|XX|Z \rangle$ and $\langle \overline{Z}|XY|Z \rangle$ spectra [Figs. 3(b) and 3(c)].

A number of additional peaks are detected in the scattering spectra at 139, 154, 165, 250, 262, 304, 324, 357, 373, and 418 cm^{-1}. They are not marked in Fig. 3(a) to avoid
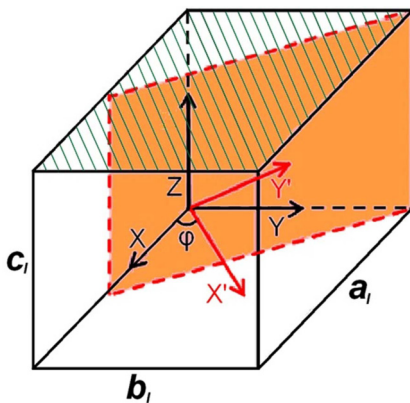
FIG. 2. (Color online) Orthorhombic crystal lattice with indication of two crystal planes and selected coordinates systems: (0 0 1) plane (hatched) with (X Y Z) system and (2 1 0) plane (orange) with ($X'Y'Z$) system.

overloading of the graph, but some of them are well resolved in Figs. 3(b) and 3(c). In most of the cases, their intensity variation upon scattering configuration is consistent with that expected for an A_1 symmetry mode, but there are no corresponding calculated first-order lines. Taking into account the rather large number of phonon branches of various symmetry in the wurtzstannite structure, it is reasonable to assume that these additional modes are due to two phonon scattering processes; they are marked as 2P in Figs. 3(b) and 3(c). Furthermore, close proximity of these two-phonon modes to one-phonon modes of identical symmetry could lead to a significant increase of their intensity due to their interaction [31]. This fact could be responsible for the absence of two-phonon bands in the spectral range above 420 cm^{-1}, where there are no one-phonon modes. It is also important to mention that the full width at half maximum (FWHM) of the majority of 2P peaks is nearly double in comparison with those of the peaks identified with one-phonon modes. This supports the interpretation that these 2P peaks are due to two-phonon modes.

In principle, presence of secondary phases and/or defects could also cause additional contributions in the spectra, leading to the observed 2P peaks. However, no evidence from presence of secondary phases has been obtained by XRD from the high crystalline quality single crystals used in this investigation. In addition, the FWHM of the most intense peak is as low as 5–6 cm^{-1}, which strongly suggests the absence of significant defect-induced effects in the spectra. All this supports the interpretation proposed in the previous paragraph for the 2P peaks as due to two-phonon modes.

The most intense Raman band at 360 cm^{-1} is asymmetrically broadened towards lower frequency. In Figs. 3(b) and 3(c), we used two Lorentzian peaks centered at 362 cm^{-1} and 357 cm^{-1} to fit this mode. As mentioned above, the lower peak at 357 cm^{-1} was associated with the two-phonon process. An alternative explanation for this asymmetric shape of the most intense Raman peak at 360 cm^{-1} could be due to the existence of disorder effects because of the presence of struc-

TABLE III. Raman scattering intensities for selected scattering configurations from the two planes of wurtzstannite-type crystals.

Modes	Plane (2 1 0)			Plane (0 0 1)	
	$\langle \overline{X'}|ZZ|X' \rangle$	$\langle \overline{X'}|ZY'|X' \rangle$	$\langle \overline{X'}|Y'Y'|X' \rangle$	$\langle \overline{Z}|XX|Z \rangle$	$\langle \overline{Z}|XY|Z \rangle$
A_1(TO+LO)	$|c|^{2a}$	0	$|(a+3b)/4|^{2a}$	$|a|^{2b}$	0
A_2	0	0	$\left|\sqrt{3}d/2\right|^2$	0	$|d|^2$
B_1(TO+LO)	0	$|e/2|^2$	0	0	0
B_2(TO+LO)	0	$\left|\sqrt{3}f/2\right|^2$	0	0	0

[a]Only TO components are allowed in the plane (2 1 0).
[b]Only LO components are allowed in the plane (0 0 1).

tural defects in the crystal, as has been recently reported for the main peaks from $Cu_2ZnSnSe_4$ [32] and Cu_2ZnSnS_4 [33,34]. However, the previous reports [32,33] deal with polycrystalline thin film samples that were synthesized under conditions that can lead to a significant content of structural defects and secondary phases. In addition, in Ref. [34] the investigated samples were single crystals grown by the Bridgman method, which lead to crystal regions with poorer crystalline quality that were characterized by a strong increase of the lower frequency contribution that becomes even dominant in the experimental spectra. This contrasts with the higher crystalline quality of the samples investigated in this work that were obtained by the chemical vapor transport technique. Because of the better crystal quality of the samples, we assume a two-phonon nature for the $357\ cm^{-1}$ mode, which, for instance, might be a result of the two-phonon combination of the $178\ cm^{-1}$ mode. In this case, a two-phonon combination presents a fully symmetrical excitation, which in turn can be enhanced by the next strongest mode at $362\ cm^{-1}$. Additional support for this interpretation of the asymmetry of the $360\ cm^{-1}$ Raman band is given from the RR spectra measured at 80 K, as discussed in Sect. IV.C.

Finally, an estimation has been made on the values of the Raman tensor elements of the main A_1(TO) mode at $361\ cm^{-1}$. The intensity of this peak measured from the (2 1 0) crystal plane has different values for the two parallel configurations: $|c|^2$ at $\langle \overline{X'}|ZZ|X' \rangle$ and $|(a+3b)/4|^2$ at $\langle \overline{X'}|Y'Y'|X' \rangle$ (Table III). Comparing the corresponding experimental spectra gives $|(a+3b)/4c|^2 \approx 1$. Values of this ratio close to 1 have also been observed for the main A_1(TO) modes of orthorhombic Cu_2ZnSiS_4 and $Cu_2ZnSiSe_4$ [25], which seems to be a characteristic property of this class of quaternary compounds.

B. B symmetry modes

Among accessible experimental scattering configurations, both B_1 and B_2 symmetry modes are active only in $\langle \overline{X'}|ZY'|X' \rangle$ spectra so that they could not be experimentally discriminated (Table III). From the spectrum shown in Fig. 4, we identified only three modes that could be assigned to the B symmetry, corresponding to the peaks at 111, 175, and $376\ cm^{-1}$. The identification of other B symmetry modes was compromised by the presence in the spectrum of a rather strong background from A_1 symmetry modes, even if in
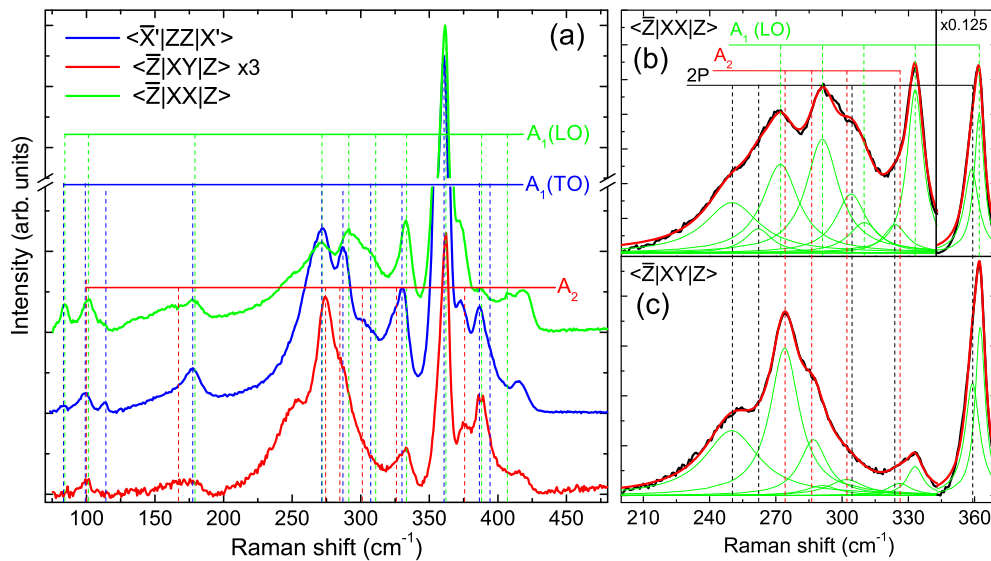
FIG. 3. (Color online) (a) Polarized Raman spectra of Cu_2ZnGeS_4 measured in different scattering configurations. (b), (c) Enlarged spectral region of the most intensive peaks (black lines) with fitting to Lorentzian curves (green lines) and cumulative peak (red lines).
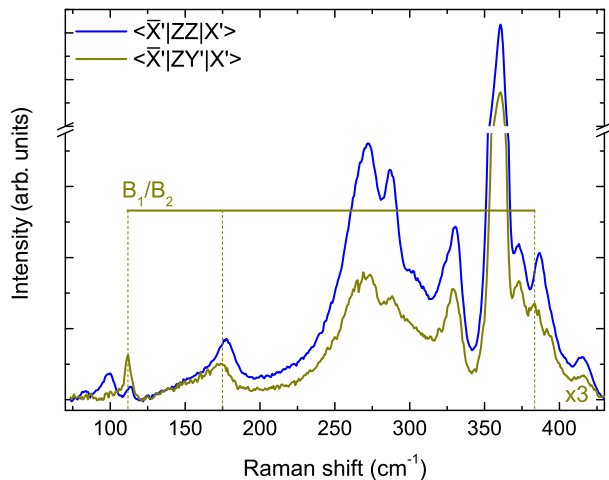
FIG. 4. (Color online) Polarized Raman spectra of Cu_2ZnGeS_4 measured in different configurations from the (2 1 0) plane.

principle these modes are forbidden in this configuration. This, together with the low intensity of the B modes, has not allowed detection of other B symmetry modes. Presences of this intense "forbidden" background from A_1 modes could only partly be a result of non-ideal measurement conditions such as incomplete polarization of incident and scattered beams, tilt sample, etc. In view of earlier reported experimental data for wurtzstannite materials [25], this is apparently a general feature of these compounds.

In principle, observation of forbidden modes in polarization Raman scattering configurations could also take place for B symmetry modes. Identification of the main B symmetry modes is made working with $\langle \overline{X'}|ZY'|X' \rangle$ configuration, where they have the highest intensity. However, experimentally, we have not observed a background contribution from these modes in the other polarization configurations. This supports the previous identification of the modes detected with the other configurations with $A_1(TO+LO)$ and A_2 symmetry modes, as discussed in Sect. IV.A. Polarization measurements under different azimuth angles—that are beyond the scope of this paper—will clarify this assignment, mainly for the low intensity peaks.

In Table II the three experimentally observed peaks are assigned to B_1 symmetry modes based on their closeness to calculated mode frequencies. We have to mention, however, that the 111 cm^{-1} experimental mode could be due to DFT-calculated B_2 symmetry mode at 106 cm^{-1}; in this sense, the assignment of this mode is only tentative.

C. RR scattering

As mentioned previously, some of the observed modes were assumed to be due to second-order scattering processes. To clarify this fact, it is instructive to compare spectra measured in nonresonant and resonant conditions at room and liquid nitrogen temperatures from the (0 0 1) plane. In the room temperature nonresonant spectrum (upper curve in Fig. 5), one observes almost all $A_1(LO)$ modes, which were identified from polarization measurements. At the same time one can notice the presence of weaker A_2 symmetry modes. This is clearly
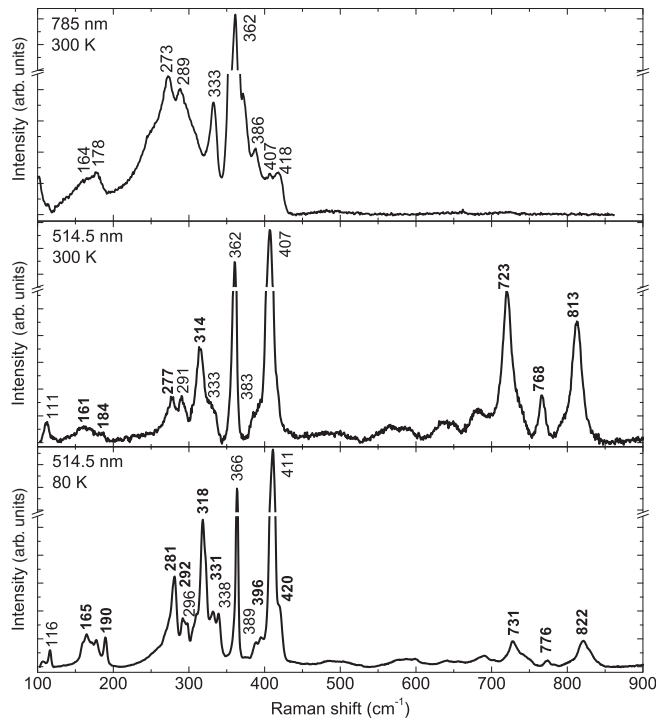
FIG. 5. Unpolarized Raman spectra of Cu_2ZnGeS_4 measured under nonresonant (top, 785 nm laser line) and resonant (514.5 nm laser line) conditions at 300 K (middle) and 80 K (bottom) from the (0 0 1) plane. Position of the most intense peaks is indicated. Peaks that appear only in the resonant spectra are indicated with bold numbers.

seen for the peak at 289 cm^{-1} in the nonresonant spectra, where comparable contribution from $A_1(LO)$ at 291 cm^{-1} and A_2 at 287 cm^{-1} modes results in the location of the maximum of the experimental peak at 289 cm^{-1} between these two modes. In the RR spectra, due to higher intensity of the $A_1(LO)$ with respect to the A_2 peak one observes a peak at 291 cm^{-1}.

Further, there are dramatic changes of the relative intensity of the peaks located at higher wavenumbers. In particular, the 407 cm^{-1} A_1 mode clearly shows an increase of its relative intensity in resonant conditions (the middle spectrum in Fig. 5). Here it is important to note that mode at 407 cm^{-1} is the one among A_1 modes with the highest TO-LO splitting found both theoretically and experimentally (see Table II). Earlier similar peculiarities of RR spectra have been documented for multicomponent $A^{II}B^{VI}$ semiconductors possessing several TO-LO branches with different ionicity [35]. In both cases higher ionicity of a particular vibrational mode (and larger TO-LO splitting) seems to be responsible for more pronounced enhancement of the intensity of the Raman line under resonant conditions.

The longitudinal nature of the two intense high frequency modes at 362 and 407 cm^{-1} in RR spectra was also confirmed by clear observation [36,37] of the second-order scattering lines (overtones at 723 cm^{-1}, 813 cm^{-1}, and their combination at about 768 cm^{-1}). Some additional modes were also detected at 161, 184, 277, and 314 cm^{-1}. In the spectra obtained at 80 K, the intensity of all these modes was enhanced. We

attributed these modes to the closest calculated B symmetry modes in Table II, but this assignment is only tentative. Note that breaking of symmetry selection rules, like the appearance of forbidden LO components of polar modes (in our case B modes in (0 0 1) plane), was previously observed in $A^{II}B^{VI}$ compounds [38] in resonant conditions. In the case of Cu_2ZnGeS_4, modes that show especially strong resonant enhancement are located at 292, 331, 396, and 420 cm^{-1} in low temperature spectra, and we attributed them to B symmetry mode, too. As shown in Table II, agreement between the calculated frequencies and the experimental ones (according to this interpretation) is again quite acceptable, with relative differences below 5% for most of the peaks.

From the comparison of the RR spectra measured at 300 and 80 K (Fig. 3), a decrease in intensity of the second-order modes (723, 768, and 813 cm^{-1}) at lower temperature was found. Based on these observations, we analyzed the intensity of 2P peaks in the RR spectra at 80 K. Lorentzian deconvolution of the RR spectra reveals significantly lower relative intensities of the 2P peaks in comparison with the one-phonon modes. This provides additional support to the two-phonon nature attributed to the 2P peaks. It is worth mentioning that Raman band at 362 cm^{-1} (366 cm^{-1} at 80 K) narrows, and it has more symmetrical shape under resonance condition, in contrast to the previously discussed case for the nonresonance case (Fig. 3). The peak at 723 cm^{-1} also does not exhibit asymmetry shape at lower wavelength number. These observations support the interpretation of the asymmetry of the 360 cm^{-1} mode proposed in part A (Fig. 3) as due to two-phonon excitation at 357 cm^{-1}, as under resonance essentially only the longitudinal component (362 cm^{-1}) is enhanced. However, for the unambiguous identification of the observed modes, further low temperature Raman polarized measurements are required.

V. CONCLUSIONS

Polarized Raman scattering study on the (2 1 0) and (0 0 1) crystallographic planes of Cu_2ZnGeS_4 single crystals is reported. The symmetries of 29 peaks, including polar A_1(TO+LO), B_1(TO+LO), and B_2(TO+LO) and nonpolar A_2 modes, are identified from the Raman spectra obtained in different geometries via analysis of the scattering selection rules and from RR spectra. A good agreement of the observed mode frequencies with the DFT calculated lattice eigenmodes further supports the symmetry mode assignment. It is shown that under resonant conditions there is a strong enhancement of intensity of fully symmetric A_1(LO) modes.

[1] W. Schafer and R. Nitsche, Mat. Res. Bull. **9**, 645 (1974).

[2] A. F. Moodie and H. J. Whitfield, Acta Cryst. B **42**, 236 (1986).

[3] K. Doverspike, K. Dwight, and A. Wold, Chem. Mater. **2**, 194 (1990).

[4] H. Matsushita, T. Ichikawa, and A. Katsui, J. Mater. Sci. Lett. **40**, 2003 (2005).

[5] O. V. Parasyuk, L. V. Piskach, Y. E. Romanyuk, I. D. Olekseyuk, V. I. Zaremba, and V. I. Pekhnyo, J. Alloys Compd. **397**, 85 (2005).

[6] Y. Shapira, E. J. McNiff, N. F. Oliveira, E. D. Honig, K. Dwight, and A. Wold, Phys. Rev. B **37**, 411 (1988).

[7] O. W. Shih, R. L. Aggarwal, T. Q. Vu, Y. Shapira, K. Doverspike, R. N. Kershaw, K. Dwight, and A. Wold, Phys. Rev. B **45**, 14025 (1992).

[8] I. Tsuji, Y. Shimodaira, H. Kato, H. Kobayashi, and A. Kudo, Chem. Mater. **22**, 1402 (2010).

[9] G. M. Ford, Q. Guo, R. Agrawal, and H. W. Hillhouse, Chem. Mater. **23**, 2626 (2011).

[10] C. J. Hages, S. Levcenco, C. K. Miskin, J. H. Alsmeier, D. Abou-Ras, R. G. Wilks, M. Bär, T. Unold, and R. Agrawal, Prog. Photovolt: Res. Appl., doi:10.1002/pip.2442 (2013).

[11] S. Chen, A. Walsh, J.-H. Yang, X. G. Gong, L. Sun, P. X. Yang, J. H. Chu, and S.-H. Wei, Phys. Rev. B **83**, 125201 (2011).

[12] Q. Shu, J. H. Yang, S. Chen, B. Huang, H. Xiang, X. G. Gong, and S.-H. Wei, Phys. Rev. B **87**, 115208 (2013).

[13] S. Chen, X. G. Gong, A. Walsh, and S.-H. Wei, Phys. Rev. B **79**, 165211 (2009).

[14] J. Paier, R. Asahi, A. Nagoya, and G. Kresse, Phys. Rev. B **79**, 115126 (2009).

[15] D. Chen and N. M. Ravindra, J. Alloys Comp. **579**, 468 (2013).

[16] N. B. Mortazavi Amiri and A. Postnikov, Phys. Rev. B **82**, 205204 (2010).

[17] T. Gurel, C. Sevik, and T. Cagın, Phys. Rev. B **84**, 205201 (2011).

[18] S. Chen, A. Walsh, Y. Luo, J.-H. Yang, X. G. Gong, and S.-H. Wei, Phys. Rev. B **82**, 195203 (2010).

[19] S. Levcenco, D. O. Dumcenco, Y. S. Huang, K. K. Tiong, and J. D. Wu, Optical Materials **34**, 183 (2011).

[20] M. Leon, S. Levcenko, R. Serna, G. Gurieva, A. Nateprov, J. M. Merino, E. J. Friedrich, U. Fillat, S. Schorr, and E. Arushanov, J. Appl. Phys. **108**, 093502 (2010).

[21] S. Levcenko, M. Guc, C. Merschjann, G. Gurieva, S. Schorr, M. Lux-Steiner, and E. Arushanov, Phys. Status Solidi C **10**, 1079 (2013).

[22] M. Himmrich and H. Haeuseler, Spectrochimica Acta A **47**, 933 (1991).

[23] M. Guc, V. Izquierdo-Roca, A. Pérez Rodríguez, G. Gurieva, S. Levcenko, S. Schorr, and E. Arushanov, Phys. Status Solidi C **10**, 1075 (2013).

[24] G. Pezzotti, J. Appl. Phys. **113**, 211301 (2013).

[25] M. Guc, S. Levcenko, V. Izquierdo-Roca, X. Fontane, M. Ya. Valakh, E. Arushanov, and A. Pérez-Rodríguez, J. Appl. Phys. **114**, 173507 (2013).

[26] M. Guc, S. Levcenko, V. Izquierdo-Roca, X. Fontane, E. Arushanov, and A. Pérez-Rodríguez, J. Appl. Phys. **114**, 193514 (2013).

[27] J. P. Perdew, K. Burke, and M. Ernzerhof, Phys. Rev. Lett. **77**, 3865 (1996).

[28] S. J. Clark, M. D. Segall, C. J. Pickard, P. J. Hasnip, M. I. J. Probert, and K. Z. Refson, Z. Kristallogr. **220**, 567 (2005).

[29] K. Refson, P. R. Tulip, and S. J. Clark, Phys. Rev. B **73**, 155114 (2006).

[30] R. Loudon, Adv. Phys. **13**, 423 (1964).

[31] M. Ya. Valakh, M. P. Lisitsa, G. S. Pekar, G. N. Polysskii, V. I. Sidorenko, and A. M. Yaremko, Phys. Status Solidi B **113**, 635 (1982).

[32] R. Djemour, A. Redinger, M. Mousel, L. Gütay, X. Fontané, V. Izquierdo-Roca, A. Pérez-Rodríguez, and S. Siebentritt, Opt. Express **21**, A695 (2013).

[33] M. Dimitrievska, A. Fairbrother, A. Pérez-Rodríguez, E. Saucedo, and V. Izquierdo-Roca, Acta Materialia **70**, 272 (2014).

[34] M. Y. Valakh, O. F. Kolomys, S. S. Ponomaryov, V. O. Yukhymchuk, I. S. Babichuk, V. Izquierdo-Roca, E. Saucedo, A. Perez-Rodriguez, J. R. Morante, S. Schorr, and I. V. Bodnar, Phys. Status Solidi RRL **7**, 258 (2013).

[35] M. Ya. Valakh and A. P. Litvinchuk, Fiz. Tverd. Tela **27**, 1958 (1985).

[36] J. F. Scott, R. C. C. Leite, and T. C. Damen, Phys. Rev. **188**, 1285 (1969).

[37] M. Ya. Valakh, A. P. Litvinchuk, G. S. Pekar, and G. N. Polisskii, Fiz. Tevrd. Tela **23**, 1010 (1981).

[38] P. Yu and M. Cardona, *Fundamentals of Semiconductors*, Third Edition (Springer, Berlin, 2002).